

Solid-state electron spin lifetime limited by phononic vacuum modes

T. Astner,^{1,*} J. Gugler,² A. Angerer,¹ S. Wald,¹ S. Putz,^{1,3} N. J. Mauser,⁴ M. Trupke,^{1,5}
H. Sumiya,⁶ S. Onoda,⁷ J. Isoya,⁸ J. Schmiedmayer,¹ P. Mohn,² and J. Majer^{9,†}

¹Vienna Center for Quantum Science and Technology,
Atominstitut, TU Wien, Stadionallee 2, 1020 Vienna, Austria

²Institute of Applied Physics, TU Wien, Wiedner Hauptstraße 8-10/134, 1040 Vienna, Austria

³Department of Physics, Princeton University, Princeton, NJ 08544, USA

⁴Wolfgang Pauli Institute c/o Faculty of Mathematics,
Univ. Wien, Oskar Morgensternplatz 1, 1090 Vienna, Austria

⁵Quantum Optics, Quantum Nanophysics & Quantum Information,
Faculty of Physics, Univ. Wien, Boltzmannngasse 5, 1090 Vienna, Austria

⁶Sumitomo Electric Industries Ltd., Itami, Hyogo, 664-0016, Japan

⁷National Institutes for Quantum and Radiological Science and Technology,
1233 Watanuki, Takasaki, Gunma 370-1292, Japan

⁸Research Centre for Knowledge Communities, University of Tsukuba, 1-2 Kasuga, Tsukuba, Ibaraki 305-8550, Japan

⁹Vienna Center for Quantum Science and Technology,
Atominstitut c/o Faculty of Mathematics, Univ. Wien,
Oskar Morgensternplatz 1, 1090 Vienna, Austria

(Dated: June 30, 2017)

Longitudinal relaxation is the process by which an excited spin ensemble decays into its thermal equilibrium with the environment. In solid-state spin systems relaxation into the phonon bath usually dominates over the coupling to the electromagnetic vacuum. In the quantum limit the spin lifetime is determined by phononic vacuum fluctuations. However, this limit was not observed in previous studies due to thermal phonon contributions or phonon-bottleneck processes. Here we use a dispersive detection scheme based on cavity quantum electrodynamics (cQED) to observe this quantum limit of spin relaxation of the negatively charged nitrogen vacancy (NV^-) centre in diamond. Diamond possesses high thermal conductivity even at low temperatures, which eliminates phonon-bottleneck processes. We observe exceptionally long longitudinal relaxation times T_1 of up to 8 h. To understand the fundamental mechanism of spin-phonon coupling in this system we develop a theoretical model and calculate the relaxation time *ab initio*. The calculations confirm that the low phononic density of states at the NV^- transition frequency enables the spin polarization to survive over macroscopic timescales.

The longitudinal relaxation of electron spins trapped in insulating solids has extensively been studied in the past - both theoretically [1–5] and in experiment [6–13]. A theoretical treatment of spin-lattice interaction results in two-phonon Raman [14] and Orbach [4] processes, dominating at higher temperatures and a direct single phonon process in the low temperature regime. If all thermal phonons are frozen out the ultimate limit of spin lifetime is given by the coupling of the spin system to the phononic vacuum modes. The observation of this limit can be obscured by a phonon bottleneck [15–17], where excited spins decay and are re-excited if the local phonon excitations are not transferred out of the system sufficiently rapid.

A suitable spin system to observe the coupling to phononic vacuum modes is the NV^- centre in diamond. Diamond has a high thermal conductivity even at low temperatures [18] which suppresses bottleneck processes. The ground state spin triplet of the NV^- centre is split due to dipolar spin-spin interaction by a zero-field splitting of $\omega_s/2\pi = D/h = 2.88$ GHz at low temperatures [19, 20] into two upper ($m_s = \pm 1$) and a lower ($m_s = 0$) level [19, 21]. With a base temperature of ~ 25 mK, our experimental apparatus can reach temperatures at which

the thermal phonon occupation ($\bar{n} \sim e^{-5.5} \approx 4 \times 10^{-4}$) at the spin transition frequency is mostly suppressed (138 mK $\hat{=}$ 2.88 GHz).

To investigate the spin-lattice interaction in this system we employ a cQED [22–25] protocol where we couple the spins to the oscillating electromagnetic field of a resonator to non-perturbatively read out the spin state as illustrated in Fig. 1a. The interaction of a spin-ensemble with the resonator mode is described by a modified Tavis-Cummings Hamiltonian [26] for a three level system with two degenerate excited states (see Methods). In the dispersive limit the resonator frequency $\omega_c/2\pi$ and the spin transition frequency $\omega_s/2\pi$ have a detuning that is much larger than the collective coupling g_N of the spin ensemble to the resonator mode ($\delta = \omega_c - \omega_s \gg g_N$). In our experiments we maintain a detuning $\delta/2\pi > 100$ MHz, corresponding to a negligible enhancement of the single spin spontaneous emission rate due to the Purcell effect [27, 28] of $\Gamma_p \approx 10^{-14} \text{ s}^{-1}$. The dispersive coupling results in a state dependent shift χ of the resonator frequency given by

$$\chi(t, T) = \frac{Ng_0^2}{\delta} (2 - 3 \langle S_z^2(t, T) \rangle). \quad (1)$$

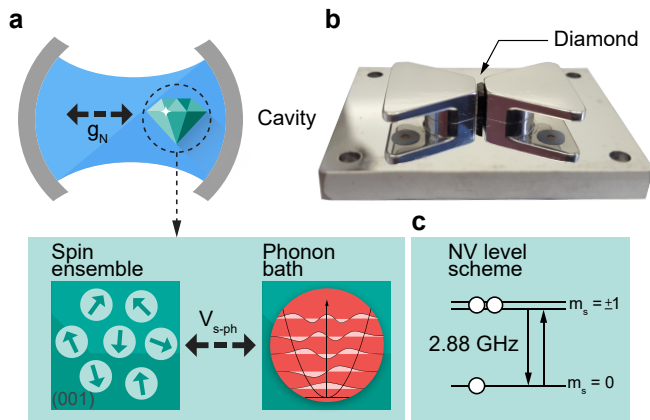


FIG. 1. Experimental set-up for measuring spin relaxation. **a**, The NV^- spin ensemble in the diamond crystal exchanges energy with the phonon bath via the spin-phonon interaction potential V_{s-ph} . The state of the spin ensemble is read out by coupling the spins dispersively to a cavity with a rate g_N . **b**, Photograph of the superconducting 3D lumped element resonator (top lid removed) with the diamond sample (black). The sample is placed between the metal structures where the magnetic field is homogeneous and all spins couple with the same coupling strength to the resonator mode. **c**, NV^- ground state spin triplet where the $m_s = \pm 1$ and $m_s = 0$ states show a zero field splitting of 2.88 GHz.

The induced shift χ is enhanced by using a large ensemble of N spins coupled to the resonator mode with a rate [29] $g_N = g_0\sqrt{N}$ and a single spin coupling rate of $g_0 \approx 38$ mHz. The expectation value $\langle S_z^2 \rangle$ is the measure for the population of spins in the excited $m_s = \pm 1$ states. Therefore, we can continuously monitor the state of the ensemble by probing the cavity resonance frequency [14, 30]. To measure the relaxation time T_1 we prepare an excited state of the ensemble and monitor the time evolution of the resonator frequency shift χ until the ensemble equilibrates with the phonon bath. Fig. 1a illustrates our system where the excited spin ensemble exchanges energy with the phonon bath.

The photograph in Fig. 1b shows how the experiment is set-up by bonding a diamond sample into a superconducting 3D lumped element resonator [31] fabricated out of aluminium with a fundamental resonance frequency $\omega_c/2\pi = 3.04$ GHz and a quality factor $Q = 60000$. The resonator geometry focuses the electromagnetic field such that all spins couple homogeneously to the resonator mode. This ensures that spin diffusion effects are negligible in contrast to 2D planar resonator designs [25]. The diamond loaded resonator is mounted in an adiabatic demagnetization refrigerator, with temperature regulation between 50 mK and 400 mK or a dilution refrigerator for temperatures below 50 mK.

As presented in Fig. 2b-c, we measure spin relaxation by first initializing our spin system in a thermal steady

state at 2.7 K, a temperature much larger than the transition energy of our system ($k_B T \gg \hbar\omega_s$). This is equivalent to $\langle S_z^2(T \gg \hbar\omega_s/k_B) \rangle_{st} \approx 2/3$. Next, we non-adiabatically switch ($\tau_{switch} \ll T_1$) to a lower target temperature to create a non-equilibrium state of the ensemble (see Methods for details of the temperature regulation). The time evolution of this state is then given by [15]

$$\frac{d}{dt} \langle S_z^2(t, T) \rangle = -\frac{1}{T_1} (\langle S_z^2(t, T) \rangle - \langle S_z^2(T) \rangle_{st}), \quad (2)$$

with

$$\langle S_z^2(T) \rangle_{st} = \frac{2}{e^{\frac{\hbar\omega_s}{k_B T}} + 2}, \quad (3)$$

as the temperature dependent steady state of $\langle S_z^2(t, T) \rangle$. We monitor its time evolution via the resonator frequency shift χ (see Eq. (1)) until a thermal equilibrium of $\langle S_z^2(t, T) \rangle$ is reached. This sequence is repeated for several different target temperatures.

A typical set of experimentally obtained $\langle S_z^2(t, T) \rangle$ versus time measurements depicted in Fig. 2a shows, that an initially prepared non-equilibrium state decays exponentially to its thermal equilibrium value $\langle S_z^2(t \rightarrow \infty, T) \rangle = \langle S_z^2(T) \rangle_{st}$ with a characteristic time T_1 .

In Fig. 3a we plot the temperature dependence of the relaxation rate $\Gamma = 1/T_1$. For temperatures above the spin transition energy $T > \hbar\omega_s/k_B$ we see a linear dependence of the relaxation rate on temperature. This corresponds to a regime where a direct, single-phonon process dominates. At temperatures $T < \hbar\omega_s/k_B$ we enter a regime where the relaxation rate is independent of temperature.

To investigate the influence of lattice damage and NV^- density on the spin phonon coupling in our system, we perform the same experiment for four different samples. We choose samples that differ in NV^- densities and the type of irradiation to create vacancies in the diamond crystal (see Table I). Samples irradiated by neutrons show much higher lattice damage than electron irradiated ones [32]. In the case of electron irradiation the generated lattice damage depends on the used electron energy and irradiation rate (this can also be seen by comparing sample E3 with E1 and E2 in Table I). As depicted in Fig. 3a the relaxation rate depends strongly on the lattice damage but is largely independent on the NV^- density. This observation indicates that the spin phonon coupling mechanism is intrinsic to the single NV^- centre and not a collective effect. From our experimental data we conclude that the spin-phonon coupling of NV^- centres in diamond is weak, resulting in remarkably long spin lifetimes of up to 8 h.

To understand the underlying mechanism of spin phonon coupling and the measured temperature dependence of Γ , we develop a theoretical model and perform

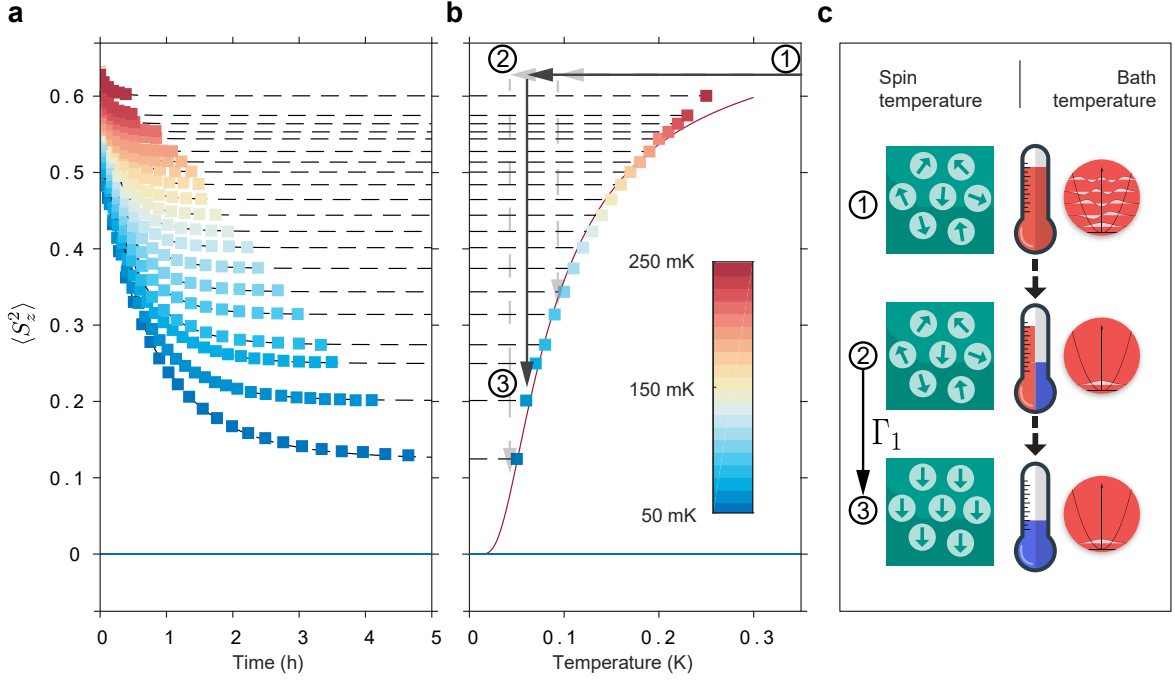


FIG. 2. **Measured time dependence and thermal steady state of $\langle S_z^2 \rangle$.** **a**, The time dependent state of the ensemble $\langle S_z^2 \rangle$ is measured by monitoring the cavity shift. To extract the relaxation rate Γ and the steady state of $\langle S_z^2 \rangle$ for a given temperature we fit an exponential decay of the form $\langle S_z^2(t, T) \rangle - \langle S_z^2(T) \rangle_{\text{st}} = (\langle S_z^2(T = 2.7\text{K}) \rangle - \langle S_z^2(T) \rangle_{\text{st}}) e^{-\Gamma t}$. The different colours of the data denote the different target temperatures. **b-c**, Temperature dependence of the steady state of $\langle S_z^2 \rangle$: we initialize the system in the steady state at 2.7 K ①. The phonon bath and the spin ensemble are in thermal equilibrium. Next we non-adiabatically switch to the target temperature ② to create a cold phonon bath but still excitations in the spin ensemble. The spin system then relaxes into its thermal equilibrium state ③ by exchanging energy with the phonon bath. The red line denotes the steady state solution of $\langle S_z^2 \rangle_{\text{st}}$ as given in eq. 3.

TABLE I. **Sample characteristics.** The samples differ in irradiation treatment, initial nitrogen concentration and final NV^- concentration and collective coupling rate g_N to the resonator mode. The residual nitrogen concentrations $[\text{N}]_{\text{initial}} - 2[\text{NV}^-]$ are estimated to be 120, 20, 24 and 180 ppm for N1, E1, E2, and E3, respectively. The measured rate of spontaneous emission Γ_0 shows a strong dependence on the method of NV^- creation. The process of sample preparation is presented in the methods section.

Sample	N1	E1	E2	E3
NV^- [ppm]	40	40	13	10
N [ppm]	≤ 200	100	50	≤ 200
Irradiation type	n	e^-	e^-	e^-
Γ_0 [s^{-1}]	$3.17 \pm 0.10 \times 10^{-4}$	$4.76 \pm 0.26 \times 10^{-5}$	$3.47 \pm 0.16 \times 10^{-5}$	$7.86 \pm 0.60 \times 10^{-5}$
g_N [MHz]	6.62 ± 0.20	9.11 ± 0.58	5.88 ± 0.20	2.85 ± 0.19
Irradiation energy [MeV]	0.1-2.5	2	2	6.5
Annealing temperature [$^\circ\text{C}$]	900	800-1000	800-1000	750-900
Irradiation dose [cm^{-2}]	9.0×10^{17}	1.1×10^{19}	5.6×10^{18}	1.0×10^{18}
Mass [mg]	19.2	44.6	22.6	10.8

ab initio calculations to quantify the relaxation rate. We consider the following mechanism [1] of spin-phonon coupling: The movement of the ions, corresponding to a phononic excitation, affects the positions of the electrons and therefore induces a change of the dipolar spin-spin interaction

$$H_{ss} = -\frac{\mu_0 g_e^2 \mu_B^2}{4\pi} \frac{(3(\mathbf{S}_i \cdot \hat{\mathbf{r}}_{ij})(\mathbf{S}_j \cdot \hat{\mathbf{r}}_{ij}) - (\mathbf{S}_i \cdot \mathbf{S}_j))}{|\mathbf{r}_{ij}|^3}. \quad (4)$$

Here μ_0 denotes the permeability of the vacuum, g_e the electronic g -factor, μ_B the Bohr-magneton, $\mathbf{S}_{i(j)}$ is the spin-vector and $\mathbf{r}_{ij}(\{\mathbf{Q}_n\})$ is the electronic distance vector, which depends on the positions of the ions. Since we are looking at small displacements, the dipolar interaction is expanded to first order with respect to the ionic positions, resulting in a perturbative potential $V_{\text{s-ph}}$ corresponding to an effective interaction which is then used in Fermi's golden rule to calculate transition rates be-

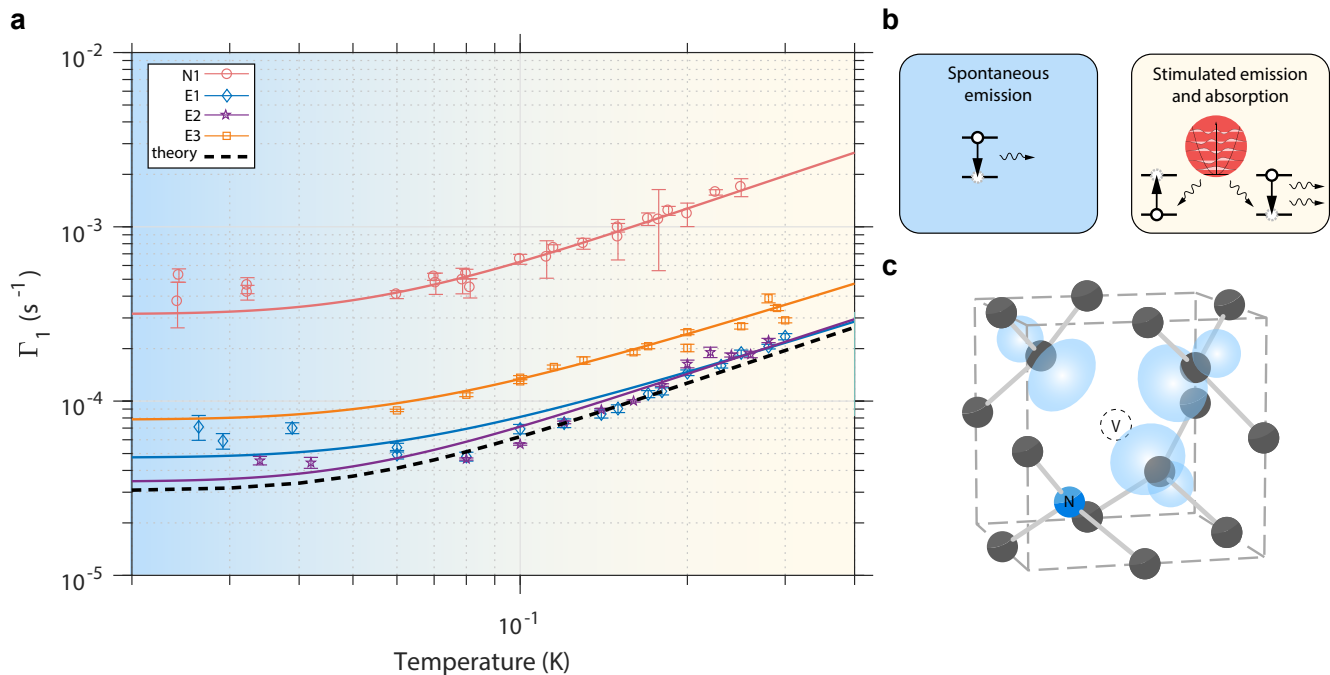


FIG. 3. **Temperature dependence of the spin-lattice relaxation rate.** **a**, The symbols represent the measured spin-lattice relaxation rates Γ for different diamond samples. We fit the theoretically predicted temperature dependence $\Gamma = \Gamma_0(1 + 3\bar{n})$ to extract the factor of proportionality Γ_0 . We find the lowest relaxation rate for an electron irradiated sample with $\Gamma_0 = 3.14 \times 10^{-5}$. Note that samples E1 and E2 with different initial nitrogen and NV^- concentration exhibit almost the same constant Γ_0 , but differ in more than one order of magnitude compared to the neutron irradiated sample N1. The dashed black line corresponds to the relaxation rate calculated *ab initio*. We identify the energy regime $k_B T < \hbar\omega_s$ (light blue background) as the quantum limit where the only remaining decay channel is spontaneous emission of a phonon. In the high energy regime $k_B T > \hbar\omega_s$ (light yellow background) the rate Γ has a linear temperature dependence. This is explained by the high temperature limit of the Bose-Einstein distribution where phonons with an energy of $\hbar\omega_s$ exist in the phonon bath. In the intermediate regime ($k_B T \approx \hbar\omega_s$) thermal phonons start to contribute to the relaxation process. **b**, Illustration of the relevant processes contributing to the spin-lattice relaxation. **c**, For illustration purposes we show the unit cell containing a single NV^- centre with the iso-surface of the spin density shown in blue. The supercell used for the calculation of the theoretical prediction plotted in **a**, is composed of 64 lattice sites including a single NV^- centre.

tween an initial and a final state $\Gamma_{f \leftarrow i}$ (see Methods section). The electronic response to the ionic motion is modelled by using the Wigner-Seitz cell as the region around the ionic equilibrium position in which the electronic orbital rigidly follows the ion. Carrying out this procedure, we end up with three relevant processes that describe the dynamics of the spin-lattice interaction in our system: A de-excitation of a spin is accompanied by spontaneous or induced emission of a phonon, whereas the absorption of a phonon excites a spin (see Fig. 3b). We perform density functional theory (DFT) calculations on a supercell with 64 lattice sites and a single NV^- centre. The diamond unit cell with a spin density iso-surface is shown in Fig. 3c. In the supercell we calculate the ionic equilibrium positions, the ionic dynamics and the electronic wavefunctions, necessary to quantify $\Gamma_{f \leftarrow i}$.

Calculating the transition rate gives us a common factor of proportionality Γ_0 for all three processes which also incorporates the phononic density of states. Spontaneous emission is temperature independent while induced emis-

sion and absorption both exhibit a temperature dependence following the Bose-Einstein distribution \bar{n} making them dominant at higher temperatures. Taking all these processes into account we end up with the differential equation (2) and derive an expression for the decay rate $\Gamma(T) = \Gamma_0(1 + 3\bar{n}(T))$. From our *ab initio* calculations we obtain the value $\Gamma_0 = 3.02 \times 10^{-5} \text{ s}^{-1}$, in agreement with our measurements for the electron irradiated crystals. These low rates are a consequence of the low phonon density of states at the spin transition energy $\hbar\omega_s$ in a diamond crystal.

Induced emission and absorption govern the linear regime of Γ which is explained by the high temperature limit of the Bose-Einstein distribution. The observed plateau at lowest temperatures stems from the temperature independent spontaneous emission of phonons where the decay rate is solely determined by the constant of proportionality Γ_0 . Since there are no thermal phonons that match the transition frequency $\omega_s/2\pi$, the measured relaxation rate is inherently limited by quantum fluctu-

ations of the phonon bath.

To conclude, we have shown through the remarkable consistency of experimental data and *ab initio* calculations that in diamond at ultra low temperatures ($T \ll \hbar\omega_s/k_B$) the longitudinal relaxation time T_1 of the electron spin is limited by the spontaneous emission of phonons into the phononic vacuum. Looking at the data in Fig. 3 one clearly can extract two main consequences: First, the irradiation and annealing process clearly distinguishes the samples. E1 and E2 (low energy electron irradiation, large dose and high temperature annealing) give T_1 identical with the *ab initio* calculations. E3 (higher energy electron irradiation with lower fluency) and N (neutron irradiation) show much more lattice damage and shorter T_1 . Second, it is remarkable that the highest and the lowest NV^- density samples have nearly identical curves, indicating that even for high densities the T_1 processes involve only single spins, and no collective effects.

Even though exceedingly long, T_1 (~ 8 h) puts a fundamental limit on the coherence time T_2 of a spin qubit in diamond. We conjecture that the observed coupling to the phononic vacuum is the dominating process determining T_1 for spin qubits in magnetically quiet insulators. Tailoring the phononic density of states using phononic meta materials such as phononic band-gaps [33] and resonators [34] may allow to engineer the spin relaxation at ultralow temperatures.

Acknowledgements

We thank W. J. Munro, J. Redinger and W. Mayr-Schmoelzer for fruitful discussions. The experimental effort has been supported by the TOP grant of TU Wien and the Japan Society for the Promotion of Science KAKENHI (No. 26246001, 26220903). T.A., A.A. and S.P. acknowledge the support by the Austrian Science Fund (FWF) in the framework of the Doctoral School Building Solids for Function (Project W1243). J.G., J.M., N.M. and P.M. acknowledge support by the FWF SFB VICOM (Project F4109-N28). J.S. and N.M. further acknowledge support by the WWTF project SEQUEX (Project MA16-066).

* thomas.astner@tuwien.ac.at

† johannes@majer.ch

- [1] Waller, I. Über die Magnetisierung von paramagnetischen Kristallen in Wechselfeldern. *Zeitschrift für Physik* **79**, 370–388 (1932).
- [2] Elliott, R. J. Theory of the Effect of Spin-Orbit Coupling on Magnetic Resonance in Some Semiconductors. *Phys. Rev.* **96**, 266–279 (1954).
- [3] Yafet, Y. g Factors and Spin-Lattice Relaxation of Conduction Electrons. *Solid State Physics - Advances in Research and Applications* **14**, 1–98 (1963).
- [4] Orbach, R. Spin-Lattice Relaxation in Rare-Earth Salts. *Proceedings of the Royal Society A: Mathematical, Physical and Engineering Sciences* **264**, 458–484 (1961).
- [5] Overhauser, A. W. Paramagnetic Relaxation in Metals. *Phys. Rev.* **89**, 689–700 (1953).
- [6] Feher, G. Electron Spin Resonance Experiments on Donors in Silicon. I. Electronic Structure of Donors by the Electron Nuclear Double Resonance Technique. *Physical Review* **114**, 1219–1244 (1959).
- [7] Harrison, J., Sellars, M. J. & Manson, N. B. Measurement of the optically induced spin polarisation of N-V centres in diamond. *Diamond and Related Materials* **15**, 586–588 (2006).
- [8] Tyryshkin, A. M. *et al.* Electron spin coherence exceeding seconds in high-purity silicon. *Nature Materials* **11**, 143–147 (2011).
- [9] Jarmola, A., Acosta, V. M., Jensen, K., Chemerisov, S. & Budker, D. Temperature- and magnetic-field-dependent longitudinal spin relaxation in nitrogen-vacancy ensembles in diamond. *Phys. Rev. Lett.* **108**, 1–5 (2012).
- [10] Mrózek, M. *et al.* Longitudinal spin relaxation in nitrogen-vacancy ensembles in diamond. *EPJ Quantum Technol.* (2015).
- [11] Culvahouse, J. W., Unruh, W. P. & Brice, D. K. Direct Spin-Lattice Relaxation Processes. *Phys. Rev.* **129**, 2430–2440 (1963).
- [12] Wu, M., Jiang, J. & Weng, M. Spin dynamics in semiconductors. *Physics Reports* **493**, 61–236 (2010).
- [13] Baral, A., Vollmar, S., Kaltenborn, S. & Schneider, H. C. Re-examination of the Elliott-Yafet spin-relaxation mechanism. *New Journal of Physics* **18**, 023012 (2016).
- [14] Schuster, D. I. *et al.* Resolving photon number states in a superconducting circuit. *Nature* **445**, 515–518 (2007).
- [15] Scott, P. L. & Jeffries, C. D. Spin-Lattice Relaxation in Some Rare-Earth Salts at Helium Temperatures; Observation of the Phonon Bottleneck. *Phys. Rev.* **127**, 32–51 (1962).
- [16] Tesi, L. *et al.* Giant spinphonon bottleneck effects in evaporable vanadyl-based molecules with long spin coherence. *Dalton Trans.* **45**, 16635–16643 (2016).
- [17] Ruby, R. H., Benoit, H. & Jeffries, C. D. Paramagnetic resonance below 1K: Spin-lattice relaxation of Ce³⁺ and Nd³⁺ in lanthanum magnesium nitrate. *Phys. Rev.* **127**, 51–56 (1962).
- [18] Slack, G. A. Thermal conductivity of pure and impure silicon, silicon carbide, and diamond. *Journal of Applied Physics* **35**, 3460–3466 (1964).
- [19] Ivády, V., Simon, T., Maze, J. R., Abrikosov, I. a. & Gali, A. Pressure and temperature dependence of the zero-field splitting in the ground state of NV centers in diamond: A first-principles study. *Phys. Rev. B* **90**, 235205 (2014).
- [20] Doherty, M. W. *et al.* Temperature shifts of the resonances of the NV-center in diamond. *Phys. Rev. B* **90**, 1–5 (2014).
- [21] Jelezko, F. & Wrachtrup, J. Single defect centres in diamond: A review. *Physica Status Solidi (a)* **203**, 3207–3225 (2006).
- [22] Mabuchi, H. Cavity Quantum Electrodynamics: Coherence in Context. *Science* **298**, 1372–1377 (2002).
- [23] Xiang, Z. Z.-L., Ashhab, S., You, J. J. & Nori, F. Hybrid quantum circuits: Superconducting circuits interacting with other quantum systems. *Rev. Mod. Phys.* **85**, 623–653 (2013).
- [24] Kubo, Y. *et al.* Hybrid Quantum Circuit with a Super-

- conducting Qubit Coupled to a Spin Ensemble. *Phys. Rev. Lett.* **107**, 220501 (2011).
- [25] Amsüss, R. *et al.* Cavity QED with Magnetically Coupled Collective Spin States. *Phys. Rev. Lett.* **107**, 060502 (2011).
- [26] Tavis, M. & Cummings, F. Exact solution for an N-moleculeradiation-field Hamiltonian. *Phys. Rev.* **170** (1968).
- [27] Purcell, E. M. Spontaneous emission probabilities at radio frequencies. *Phys. Rev.* **69**, 674–674 (1946).
- [28] Bienfait, A. *et al.* Controlling spin relaxation with a cavity. *Nature* **531**, 74–77 (2015).
- [29] Dicke, R. Coherence in spontaneous radiation processes. *Phys. Rev.* **24** (1954).
- [30] Brune, M. *et al.* From Lamb shift to light shifts: Vacuum and subphoton cavity fields measured by atomic phase sensitive detection. *Phys. Rev. Lett.* **72**, 3339–3342 (1994).
- [31] Angerer, A. *et al.* Collective strong coupling with homogeneous Rabi frequencies using a 3D lumped element microwave resonator. *Applied Physics Letters* **109**, 033508 (2016).
- [32] Nöbauer, T. *et al.* Creation of ensembles of nitrogen-vacancy centers in diamond by neutron and electron irradiation. *arXiv preprint arXiv:1309.0453* 12 (2013).
- [33] Safavi-Naeini, A. H. *et al.* Two-dimensional phononic-photonic band gap optomechanical crystal cavity. *Phys. Rev. Lett.* **112**, 1–5 (2014).
- [34] O’Connell, A. D. *et al.* Quantum ground state and single-phonon control of a mechanical resonator. *Nature* **464**, 697–703 (2010).
- [35] Sandner, K. *et al.* Strong magnetic coupling of an inhomogeneous nitrogen-vacancy ensemble to a cavity. *Phys. Rev. A* **85**, 053806 (2012).
- [36] Mahan, G. *Many-Particle Physics*. Physics of Solids and Liquids (Springer US, 2013).
- [37] Kresse, G. & Furthmüller, J. Efficient iterative schemes for *ab initio* total-energy calculations using a plane-wave basis set. *Phys. Rev. B* **54**, 11169–11186 (1996).
- [38] Blöchl, P. E. Projector augmented-wave method. *Phys. Rev. B* **50**, 17953–17979 (1994).
- [39] Perdew, J. P., Burke, K. & Ernzerhof, M. Generalized gradient approximation made simple. *Phys. Rev. Lett.* **77**, 3865–3868 (1996).
- [40] Gali, A., Fyta, M. & Kaxiras, E. *Ab initio* supercell calculations on nitrogen-vacancy center in diamond: Electronic structure and hyperfine tensors. *Phys. Rev. B* **77**, 155206 (2008).
- [41] Giannozzi, P. *et al.* Quantum espresso: a modular and open-source software project for quantum simulations of materials. *Journal of Physics: Condensed Matter* **21**, 395502 (2009).
- [42] Togo, A. & Tanaka, I. First principles phonon calculations in materials science. *Scr. Mater.* **108**, 1–5 (2015).
- [43] Mostofi, A. A. *et al.* An updated version of wannier90: A tool for obtaining maximally-localised wannier functions. *Computer Physics Communications* **185**, 2309 – 2310 (2014).

Methods and Materials

Spin system

The NV^- centre in diamond consists of a substitutional nitrogen atom with an adjacent carbon vacancy. In the diamond lattice the NV^- centre is oriented along four different crystallographic directions. Its ground state is a paramagnetic spin ($S = 1$) system which we describe with the spin Hamiltonian $H/h = DS_z^2$, with a zero field splitting constant $D = 2.88$ GHz [21]. In our experiment we use diamond samples which are cut along the (001) direction and placed in the resonator such that this plane is aligned parallel to the oscillating magnetic field.

System Hamiltonian

To describe the system we consider a modified Tavis-Cummings Hamiltonian [26] that accounts for the coupling to the degenerate $m_s = \pm 1$ spin states of the NV^- centre and a term for the cavity probe field with frequency ω_p and amplitude η :

$$\frac{H_{\text{sys}}}{\hbar} = \underbrace{\omega_c a^\dagger a + \omega_s S_z^2 + ig_N (a^\dagger S^- - a S^+)}_{H_{TC}} + i \underbrace{(\eta a^\dagger e^{-i\omega_p t} - \eta^* a e^{i\omega_p t})}_{H_p}, \quad (1)$$

where a/a^\dagger are the creation/annihilation operators for the cavity mode with angular frequency ω_c . The operator S_z^2 is a collective operator that gives a measure of the spin population in the $m_s = \pm 1$ state of an ensemble containing N spins:

$$S_z^2 = \frac{1}{N} \sum_j^N \sigma_{z,j}^2. \quad (2)$$

In the spin basis of the NV^- centre ($|1\rangle, |0\rangle, |-1\rangle$) we define $\sigma_z^2 = |1\rangle\langle 1| + |-1\rangle\langle -1|$, and the collective ladder operators S^\pm operators as:

$$S^\pm = \frac{1}{N} \sum_j^N \sigma_j^\pm \quad (3)$$

with $\sigma^- = |0\rangle\langle 1| + |0\rangle\langle -1|$ and $\sigma^+ = |1\rangle\langle 0| + |-1\rangle\langle 0|$.

Thermal excitations of the mode and ensemble are included similarly to [35] by adding standard Liouvillian terms to the dynamics and solving the corresponding master equation for the system:

$$\frac{d}{dt}\rho = \frac{1}{i} [H_{\text{sys}}, \rho] + \mathcal{L}[\rho]. \quad (4)$$

From the master equation we derive the equations of motion for the operators with the detunings $\Delta_s = \omega_s - \omega_p$ and $\Delta_c = \omega_c - \omega_p$:

$$\frac{d}{dt}\langle a \rangle = -i\Delta_c \langle a \rangle - ig_N \langle S^- \rangle + \eta - \kappa \langle a \rangle, \quad (5)$$

$$\frac{d}{dt}\langle S^- \rangle = -i\Delta_s \langle S^- \rangle - 2ig_N \langle a \rangle + 3ig_N \langle a \rangle \langle S_z^2 \rangle - (\gamma_\perp^* + 2\gamma_\parallel) \langle S^- \rangle, \quad (6)$$

$$\frac{d}{dt}\langle S_z^2 \rangle = -ig_N (\langle a \rangle \langle S^+ \rangle - \langle a^\dagger \rangle \langle S^- \rangle) - 2\gamma_\parallel \langle S_z^2 \rangle, \quad (7)$$

$$(8)$$

Next, we calculate the steady-state intra cavity field $\langle a \rangle_{\text{st}}$ for a thermal spin state from which we can extract the spin state dependent cavity shift χ in the form:

$$\chi(T) = \frac{Ng_0^2}{\delta} (2 - 3 \langle S_z^2(T) \rangle). \quad (9)$$

In the equations of motion we use γ_\perp^* for the collective ensemble line width and γ_\parallel for T_1 processes. Since the detuning δ between the spin transition and the cavity is an intrinsic parameter, we can calculate the collective

coupling strength g_N of the spin ensemble to the resonator mode via Eq. (9).

Samples

For the neutron sample N1 we use a commercially available type-Ib high-pressure, high-temperature (HPHT) diamond from the company Element Six Ltd. The crystal contains an initial nitrogen concentration of <200 ppm and a natural abundance of ^{13}C nuclear isotopes. The local neutron source was a TRIGA Mark II reactor of TU Wien. The sample was irradiated for 50 h with neutrons in the energy range of 0.1-2.5 MeV and a total dose of $1.8 \times 10^{18} \text{cm}^{-2}$. Next, the sample was annealed for 3 h at 900 °C. The achieved NV^- density is 40 ppm. In reference [32] (sample BS3-1b) details on the sample preparation are given.

For the electron sample E3 we use a similar raw diamond (HPHT) from element6 as in the case of N1. The crystal contains an initial nitrogen concentration of <200 ppm and a natural abundance of ^{13}C nuclear isotopes. We chose an irradiation with 6.5 MeV at temperatures of 750-900 °C with a total fluence of $1 \times 10^{18} \text{cm}^{-2}$ which results in a density of 10 ppm NV^- centre. The irradiation was done at the linear accelerator of the Istituto per la Sintesi Organica e la Fotoreattività in Bologna, Italy. Details concerning the preparation of this sample can be found in reference [32] (sample U5).

The electron samples E1 and E2 are type-Ib high-pressure, high-temperature (HPHT) diamond crystals with an initial nitrogen concentration of 100 ppm and 50 ppm, respectively. The sample E1 was irradiated with 2 MeV at 800 °C and annealed at 1000 °C multiple times. For the E2 sample the total electron dose was $1.1 \times 10^{19} \text{cm}^{-2}$ and the E1 sample received a total dose of $5.6 \times 10^{18} \text{cm}^{-2}$. The achieved NV^- densities are 40 ppm and 13 ppm respectively. The electron irradiation was performed by using a Cockcroft-Walton accelerator of the QST, Takasaki.

Microwave resonator

The superconducting 3D lumped element cavity is machined out of aluminium (EN AW 6066) and mechanically polished down to a roughness of $\approx 0.25 \mu\text{m}$ [31]. To bond the crystal samples into the resonator and ensure good thermal contact we use a small amount of vacuum grease as adhesive. We determine the fundamental resonance frequency $\omega_c/2\pi = 3.04 \text{GHz}$ and a quality factor $Q = 60000$ by transmission spectroscopy with spin transitions far detuned from the resonator mode.

Transmission measurements

In our transmission spectroscopy we determine the forward scattering parameter $|S_{21}|^2$ with a standard vector network analyser (R&S ZNB-8). After cool-down we continuously monitor the transmission to extract the time evolution of the cavity resonance. During the experiment we probe the cavity with an input power of -110dBm which corresponds to an average number of 1×10^{-9} photons/spin in the cavity.

Sample initialization procedure

We use an adiabatic demagnetization refrigerator (ADR-Rainier, HPD) with the advantage of temperature regulation in the temperature regime of interest. After measuring the relaxation time for a certain temperature the paramagnetic salt in the fridge has to be magnetized and the fridge is cycled through the 2.7 K heat bath provided by a pulse tube cooler. During this regeneration time of the magnet the spin ensemble is kept at high temperature for initialization. The cooldown time to base temperatures between 50-250 mK is in the order of 20-40 min, which is fast enough that the spins do not completely relax during the cool down process. Since the ADR is limited to 50 mK, the additional data points are measured in a standard dilution refrigerator (Oxford DR-200) where an electric heater allows to thermally initialize the spin ensemble at 1 K. Therefore, we only show a single complete data set of relaxation curves in Fig. 2 which was measured in the adiabatic demagnetization refrigerator. The additional low temperature relaxation measurements in the dilution refrigerator have a different signal amplitude but show the same exponential behaviour.

Ab initio calculation based on density functional theory

For the calculation of the electron phonon interaction, we consider the change of the electron spin-spin interaction H_{ss} with respect to the ionic movements $\{\mathbf{Q}_n\}$.

$$H_{ss}(\{\mathbf{Q}_n\}) = - \underbrace{\frac{\mu_0 g_e^2 \mu_B^2}{4\pi}}_{:=\alpha} \frac{(3(\mathbf{S}_i \cdot \hat{\mathbf{r}}_{ij}(\{\mathbf{Q}_n\}))(\mathbf{S}_j \cdot \hat{\mathbf{r}}_{ij}(\{\mathbf{Q}_n\})) - (\mathbf{S}_i \cdot \mathbf{S}_j))}{|\mathbf{r}_{ij}(\{\mathbf{Q}_n\})|^3} \quad (10)$$

Here μ_0 is the permeability of the vacuum, g_e the electronic g-factor, μ_B the Bohr-magneton, $\mathbf{S}_{i(j)}$ the spin-vector and $\mathbf{r}_{ij}(\{\mathbf{Q}_n\})$ is the electronic distance vector dependent on the positions of the ions. The electronic response to the ionic motion is modelled by defining a region around the ionic equilibrium position $\mathbf{R}_n^{(0)}$, in which the electronic orbital rigidly follows the ion. This region is chosen to be the Wigner-Seitz cell. Since we are looking at small displacements, the spin-spin interaction is expanded to first order in the ionic positions. This results in the time dependent perturbative potential V_{s-ph} , which we use in Fermis golden rule to calculate the transition rate $\Gamma_{f \leftarrow i}$:

$$\begin{aligned} \Gamma_{f \leftarrow i} &= \frac{1}{\hbar^2} \sum_f |\langle N^f, m_s^f | V_{s-ph} | N^i, m_s^i \rangle|^2 \delta(\nu = 2.88 \text{ GHz}) \\ &= \frac{\alpha^2}{\hbar^2} \sum_f |\langle m_s^f | \sum_n \sum_{i>j} \frac{3(S_i^\pm S_j^z + S_i^z S_j^\pm) (\langle N^f | (Q_n^x \mp iQ_n^y) | N^i \rangle) r_{ij}^z + (r_{ij}^x \mp ir_{ij}^y) \langle N^f | Q_n^z | N^i \rangle \Delta\Theta_{ij}^n}{2|\mathbf{r}_{ij}|^5} \\ &\quad - \frac{15(S_i^\pm S_j^z + S_i^z S_j^\pm) (r_{ij}^x \mp ir_{ij}^y) r_{ij}^z (\mathbf{r}_{ij} \cdot \langle N^f | \mathbf{Q}_n | N^i \rangle) \Delta\Theta_{ij}^n}{2|\mathbf{r}_{ij}|^7} |m_s^i\rangle|^2 \delta(\nu = 2.88 \text{ GHz}) \end{aligned} \quad (11)$$

Here $m_s^{i(f)}$ and $N^{i(f)}$ denote the initial (final) electronic and phononic states and $\Delta\Theta_{ij}^n$ accounts for the fact that the spin-spin interaction between the electronic spins is only changed if either electron i or electron j is inside the Wigner-Seitz cell of the displaced ion and the other one outside. Inserting the second quantized form of the ionic displacement [36]

$$\mathbf{Q}_n = \sum_{\mathbf{q}, \nu} \sqrt{\frac{\hbar}{2M_n N \omega_{\mathbf{q}, \nu}}} (a_{-\mathbf{q}, \nu}^\dagger + a_{\mathbf{q}, \nu}) \boldsymbol{\epsilon}_{\mathbf{q}, \nu} e^{i\mathbf{q} \cdot \mathbf{R}_n^{(0)}} \quad (12)$$

and performing the summation over the final phonon modes leads to a spin-lattice relaxation time T_1 proportional to the thermal occupation of phonon modes with a frequency of 2.88 GHz for phonon induced emission and absorption and a temperature independent contribution corresponding to spontaneous emission of a phonon with a constant of proportionality Γ_0 , dependent on the electronic wavefunctions and the phononic polarization vectors.

The NV⁻ center was simulated *ab initio* in a supercell containing 63 atoms and one vacancy with the Vienna *ab initio* simulation package (VASP [37]) using projector augmented wave (PAW) pseudopotentials [38] and the exchange-correlation potential of Perdew, Burke and Ernzerhof [39]. Plane waves up to an energy of 700 eV were considered and the Brillouin zone was sampled with a very dense mesh using 19 k-points inside the irreducible wedge. A careful relaxation of the ions to their equilibrium position showed that the nitrogen atoms relax more than the carbon atoms, in agreement with previous calculations [40]. The resulting forces were less than 1 meV/Å per atom. The results were also confirmed using the Quantum Espresso package [41]. The diagonalization of the dynamical matrix was done using the PHONOPY-package [42] and the rate $\Gamma_{f \leftarrow i}$ was calculated using maximally localized Wannier functions, obtained with WANNIER90 [43].